Actinyls in Expanded Porphyrin: A Relativistic Density-Functional Study†

Meng-Sheng Liao, Tapas Kar, and Steve Scheiner*

Department of Chemistry and Biochemistry, Utah State University, Logan, Utah 84322-0300

Received: September 30, 2003; In Final Form: January 15, 2004

Actinyls AnO_2 with An = U, Np, and Pu in an expanded porphyrin, alaskaphyrin (AP), are studied by a relativistic density-functional method. The electronic structures of both AnO_2 and AnO_2AP are investigated by considering all possible low-lying states. To examine the importance of relativity, nonrelativistic calculations were also performed. For UO_2 and NpO_2, the ground state is altered by the relativistic effects, but it remains unchanged for PuO_2. The nonrelativistic ground states of the AnO_2AP complexes are all high spin, where the AP highest occupied molecular orbital, b_{2g}, is singly occupied. At the relativistic level, there are two electrons in b_{2g}. The bonding characteristics in AnO_2AP are examined by calculations of the AnO_2-AP binding energy and charge distribution on AnO_2. Other properties such as ionization potentials and electron affinities are also calculated. The predicted spectroscopic constants for NpO_2, PuO_2, NpO_2AP, and PuO_2AP would aid in future spectroscopic studies of these molecules.

1. Introduction

Actinides (An), particularly uranium and plutonium, are important in the nuclear industry, but their production has generated severe environmental problems with huge quantities of radioactive waste. Therefore, considerable efforts have been made to develop effective complexing agents that can be used to extract the actinides from the nuclear waste. One method involves the coordination of actinides with a macrocycle. So far, the widely studied macrocyclic systems include calixarenes[1] and crown ethers.[2] In the early 1990s, Sessler et al.[3] developed a new class of pyrrole-based aromatic "expanded porphyrins" that was capable of complexing uranyl (UO_2) effectively. Later, a variety of expanded porphyrins were reported by Sessler and co-workers[4−12] to form stable complexes with actinyls (AnO_2); they include pentaphyrin, sapphyrin, alaskaphyrin, grandephyrin, hexaphyrin, and amethyrin.

Expanded porphyrins, as the name implies, are polypyrrolic macrocycles that are larger than normal, tetradentate porphyrins. Normal porphyrins (Por) are well-known as excellent complexation agents for transition metals, which has led to an explosion of experimental studies in this field. In contrast, examples of actinide porphyrins are limited[13,14] [$ThPor(acac)_2$, $MPor(Cl)_2L_2$ (M = Th, U), $UPor(Cl)_2(THF)$, $MPor_2$ (M = Th, U)] where the actinides are too large to sit within the porphyrin core, thus forming relatively unstable out-of-plane or sandwich complexes. The larger, expanded porphyrins provide a better "fit" for larger metal cations and thus appear more attractive as ligands for the specific purpose of actinyl coordination.

A suitable actinide-coordinating agent should possess the features of capturing the metal, isolating it, and rendering it insoluble in water.[12] So the rational design for such macrocycles requires a detailed understanding of the complex stability. Clearly, the ability to predict the strength and nature of the binding between the actinyl and the expanded porphyrin is of great importance and has the potential to eliminate costly experiments on toxic compounds.

This paper comprises a relativistic density-functional study of actinyl in an expanded porphyrin. As a first step in theoretical studies of this special class of metal porphyrins, we have chosen uranyl alaskaphyrin (UO_2AP, see Figure 1), as this complex exhibits a nearly planar structure.[4] Planar expanded porphyrins are interesting and rare; most expanded porphyrins are highly distorted, far from planarity. More recently,[12] it was also found that AP could coordinate neptunyl and plutonyl. For comparison among different actinyls, the calculations also include NpO_2-AP and PuO_2AP.

The theoretical description of actinide compounds poses a special challenge because the elements are large, with high nuclear charge, so they must be treated in a relativistic manner. An equally difficult problem is caused by the active role of the 5f orbitals in the bonding. In contrast to the lanthanides where the open 4f shell is mainly located within the outer valence orbitals and does not participate in chemical bonding, the 5f orbitals in actinides are more diffuse and can contribute to the bonding.[15,16] A great deal of electron correlation in high angular momentum shells[17−19] poses another challenge to theoretical research. In addition, the open 5f, 6d, and 7s shells may result in a myriad of energetically adjacent electronic states with similar properties. The large size and complexity of AnO_2AP makes it difficult to use standard ab initio methods. Fortunately, the refinement of density-functional theory (DFT) methods in recent years has made them a suitable, and sometimes preferable, alternative to ab initio approaches. There have been a number of applications of DFT methods to calculations of actinide compounds (e.g., refs 17−27). Compared to classic, normal porphyrins, theoretical studies of expanded porphyrins are very rare.[28] The main aims of this work are as follows:

(i) To provide a detailed description of electronic structures of both AnO_2 and AnO_2AP (so as to examine the modifications in the electronic structure of AnO_2 due to the AP coordination).

(ii) To investigate the strength of the binding between $AnO_2^{0/2+}$ and $AP^{0/2-}$.

(iii) To investigate the influence of relativity on the actinide compounds. This is especially interesting since the f and d

† Part of the special issue "Fritz Schaefer Festschrift".

* Author to whom correspondence should be addressed. E-mail: scheiner@cc.usu.edu.

10.1021/jp036927d CCC: $27.50
Published on Web 02/13/2004

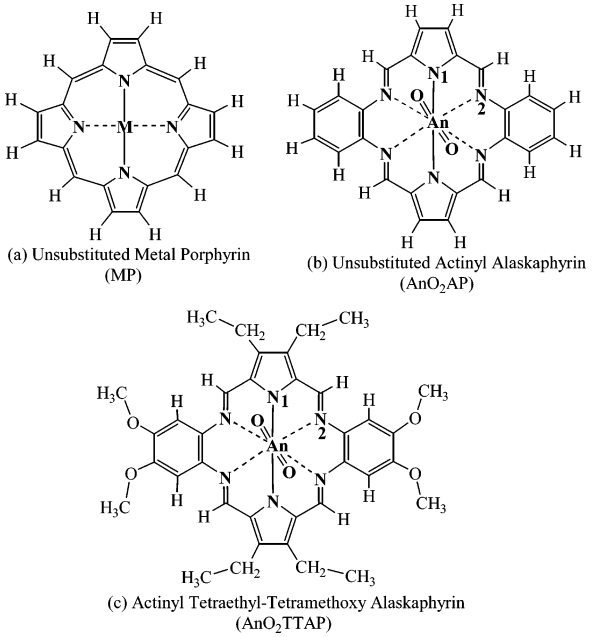

Figure 1. Molecular structures of MP, AnO_2AP, and AnO_2TTAP.

orbitals are relativistically expanded and destabilized while the s orbital is relativistically contracted and stabilized.

2. Computational Details

The molecular structure of the unsubstituted actinyl alaskaphyrin (AnO_2AP) is illustrated in Figure 1b (with the molecular structure of unsubstituted, normal metal porphyrin in Figure 1a for comparison). The systems that have been synthesized, actinyl tetraethyl-tetramethoxy alaskaphyrins AnO_2TTAP,[4,12] contain ethyl and methoxy groups as substituents on the periphery of the macrocycle ring, as shown in Figure 1c. The X-ray single-crystal structure of UO_2TTAP reveals that the uranyl is coordinated to all six nitrogen atoms in a planar fashion,[4] the maximum deviation from planarity within the macrocycle being only 0.011 Å. A planar structure for UO_2TTAP is attributed to the rigidity of the phenylene diamine ring.[5] Thus, in the calculations an idealized D_{2h} symmetry was taken for the molecular structures. For computational economy, the calculations were carried out mainly on the unsubstituted AnO_2APs. To observe the effects of the peripheral substituents on the molecular properties, results for UO_2TTAP were also calculated.

All calculations were carried out using the Amsterdam density-functional (ADF) program package (ADF 2000.02) developed by Baerends and co-workers.[29−32] The Slater-type orbital (STO) basis used for the valence shells is of triple-ζ quality, plus one polarization function for all atoms; single-ζ STOs are used for core orthogonalization. The frozen core assigned for the actinides consisted of (1s−5s), (2p−4p), (3d−5d), and 4f. It was suggested that the An 6s and 6p orbitals are flexible and cannot be considered as core orbitals.[21,22] For C/N/O the [He] core definition was used. Among the various exchange-correlation potentials available, the density-parametrization form of Vosko, Wilk, and Nusair (VWN),[33] plus Becke's gradient correction for exchange (B)[34] and Perdew's gradient correction for correlation (P),[35] were employed. It has been shown that the combined VWN-B-P functional can provide accurate bonding energies for both main-group[36] and transition metal[37] systems.

Relativistic corrections of the valence electrons were calculated by the quasi-relativistic (QR) method.[38] (The relativistic corrections of atomic cores are taken into account at the Dirac−Fock level.) In this scalar (one-component) approach, spin−orbit (SO) coupling is not taken into account. Because SO effects are mainly atomic in nature, they are not expected to have significant influence on molecular properties,[25] except metal−ligand binding energies.[15,16] To assess the magnitudes of the SO effects on the An−O bond length and AnO_2−AP binding strength, additional calculations including the SO formalism were also performed. Calculations on open-shell systems were performed using the spin-unrestricted method.

TABLE 1: Calculated Relative Energies (E) and An−O Bond Lengths (R_{An-O}) for Selected Configurations of AnO_2 and AnO_2^{2+} (An = U, Np, Pu), at Nonrelativistic (Nrel) and Relativistic (Rel) Levels

		configuration	term	E (eV)	R_{An-O} (Å)
UO_2	Nrel	$(\delta_u)^2$	$^3\Sigma_g$ (A)	0	1.776
		$(\delta_u)^1(\phi_u)^1$	^3H_g	0.21	1.785
		$(\phi_u)^2$	$^3\Sigma_g$ (B)	0.75	1.801
		$(\sigma_g)^1(\phi_u)^1$	$^3\Phi_u$	3.71	1.745
	Rel	$(\sigma_g)^1(\phi_u)^1$	$^3\Phi_u$	0	1.813
		$(\sigma_g)^1(\delta_u)^1$	$^3\Delta_u$	0.06	1.802
		$(\delta_u)^2$	$^3\Sigma_g$ (A)	0.85	1.851
		$(\delta_u)^1(\phi_u)^1$	^3H_g	0.96	1.863
		$(\phi_u)^2$	$^3\Sigma_g$ (B)	1.25	1.874
		$(\sigma_g)^2$	$^1\Sigma_g$	1.57	1.762
UO_2^{2+}	Nrel	$(\sigma_u)^2$	$^1\Sigma_g$	0	1.693
	Rel	$(\sigma_u)^2$	$^1\Sigma_g$	0	1.720
NpO_2	Nrel	$(\delta_u)^2(\phi_u)^1$	$^4\Phi_u$	0	1.766
		$(\delta_u)^1(\phi_u)^2$	$^4\Delta_u$	0.62	1.785
	Rel	$(\delta_u)^2(\sigma_g)^1$	$^4\Sigma_g$	0	1.776
		$(\delta_u)^1(\phi_u)^1(\sigma_g)^1$	^4H_g	0.01	1.791
		$(\delta_u)^2(\phi_u)^1$	$^4\Phi_u$	0.04	1.838
		$(\phi_u)^2(\sigma_g)^1$	$^4\Sigma_g$	0.35	1.806
		$(\delta_u)^1(\phi_u)^2$	$^4\Delta_u$	0.47	1.858
NpO_2^{2+}	Rel	$(\phi_u)^1$	$^2\Phi_u$	0	1.717
		$(\delta_u)^1$	$^2\Delta_u$	0.25	1.702
		$(\sigma_g)^1$	$^2\Sigma_g$	5.98	1.705
PuO_2	Nrel	$(\delta_u)^2(\phi_u)^2$	$^5\Sigma_g$	0	1.772
	Rel	$(\delta_u)^2(\phi_u)^2$	$^5\Sigma_g$	0	1.835
		$(\sigma_g)^1(\delta_u)^2(\phi_u)^1$	$^5\Phi_u$	0.25	1.770
		$(\sigma_g)^1(\delta_u)^1(\phi_u)^2$	$^5\Delta_u$	0.71	1.789
PuO_2^{2+}	Rel	$(\delta_u)^1(\phi_u)^1$	^3H_g	0	1.703
		$(\delta_u)^2$	$^3\Sigma_g$ (A)	0.21	1.687
		$(\phi_u)^2$	$^3\Sigma_g$ (B)	0.22	1.720
		$(\sigma_g)^1(\phi_u)^1$	$^3\Phi_u$	6.51	1.709
		$(\sigma_g)^1(\delta_u)^1$	$^3\Delta_u$	6.98	1.693

3. Results and Discussion

3.1. Isolated Actinyls. First reported are calculations on AnO_2 and AnO_2^{2+}, as they represent the core building block of the coordination complexes. The electronic structure and bonding of UO_2^{2+} have been the subject of much theoretical work, including some very recent calculations.[23−27] There have also been several theoretical studies of neutral UO_2.[21,22,25,39,40] In contrast, theoretical studies of other actinyls are relatively scarce.[16,23,24]

The partial occupancy of the 5f shell in the actinides may result in a number of low-lying states. To determine the ground state for the actinyls, the energetics of possible low-lying states were computed at both nonrelativistic and relativistic levels. Geometry optimization was performed for all states of each species. The relative energies of the various states in AnO_2 and AnO_2^{2+} with An = U, Np, and Pu are collected in Table 1, along with the An−O bond length of each state. Table 2a displays the calculated properties (relativistic results) for the ground state. The ionization potentials (IPs) were calculated by

TABLE 2: Calculated Properties of AnO_2 and AnO_2^{2+} (An = U, Np, Pu) in Their Ground States (Relativistic Results) and Gross Mulliken Populations (on the Atomic Orbital An-6p, ..., An-7s) and Atomic Charges (Q) on An

a: Calculated Properties of AnO_2 and AnO_2^{2+} [a]

	method	R_{An-O} (Å)	$k_{An-O}^{(s)}$ (mdyn/Å)	$\omega_{An-O}^{(s)}$ (cm^{-1})	$k_{An-O}^{(as)}$ (mdyn/Å)	$\omega_{An-O}^{(as)}$ (cm^{-1})	first IP (eV)	second IP (eV)
UO_2	ADF[b]	1.813	6.87	853	7.48	948	6.47	14.92
($^3\Phi_u$)	ADF−SO[c]	1.803	7.03	863	7.26	934		
	CASPT2[d]	1.806		809		932	6.17	14.36
	CCSD/RPP[e]							15.05
	B3LYP/RECP[f]	1.794		875		937	6.19	15.25
	B3LYP/PP[g]	1.800		874		931	6.27	15.31
	exptl					914.8[h]	6.19[i]	15.4 ± 2.6[j]
UO_2^{2+}	ADF	1.720	9.39	997	9.97	1095		
($^1\Sigma_g$)	CISD[k]	1.700		1082		1157		
	CASPT2[l]	1.728						
	CCSD(T)[l]	1.706						
	4-CCSD[m]	1.696		1040		1168		
	4-CCSD(T)[m]	1.715		974				
	B3LYP[n]	1.706		1041		1147		
NpO_2	ADF	1.773	7.11	868	6.28	869	6.43	15.74
($^4\Sigma_g$)	ADF−SO	1.778	7.15	870	6.62	892		
NpO_2^{2+}	ADF	1.717	8.86	969	9.61	1075		
($^2\Phi_u$)								
PuO_2	ADF	1.833	5.63	772	5.09	781	6.92	16.59
($^5\Sigma_g$)	ADF−SO	1.812	5.90	791	6.26	866		
PuO_2^{2+}	ADF	1.703	8.57	953	10.10	1100		
(^3H_g)	CISD+Q[o]	1.677						
	AQCC[p]	1.670		1005				
	B3LYP[n]	1.688		1014		1144		

b: Gross Mulliken Populations and Atomic Charges

	UO_2	UO_2^{2+}	NpO_2	NpO_2^{2+}	PuO_2	PuO_2^{2+}
An-6p, e	5.71	5.51	5.62	5.51	5.76	5.46
An-6d, e	1.29	1.21	1.27	1.12	1.03	1.07
An-5f, e	2.94	2.65	4.09	3.78	5.72	4.91
An-7s, e	0.65	0.00	0.63	0.00	0.00	0.00
Q_{An}, e	1.41	2.81	1.39	2.76	1.60	2.76

[a] R_{An-O} is the An−O bond length; $k_{An-O}^{(s)}$ is the symmetric An−O force constant; $\omega_{An-O}^{(s)}$ is the symmetric An−O vibrational frequency; $k_{An-O}^{(as)}$ is the antisymmetric An−O force constant; $\omega_{An-O}^{(as)}$ is the antisymmetric An−O vibrational frequency; IP is the ionization potential. [b] Present ADF calculations. [c] ADF calculations including spin−orbit (SO) coupling. [d] CASPT2 calculation with a large basis set and a large active space, ref 39a. [e] CCSD calculation with relativistic pseudopotential, ref 45. [f] B3LYP calculation with relativistic effective core potential, ref 39a. [g] B3LYP calculation with pseudopotential (PP), ref 25. [h] Reference 25. [i] Reference 43. [j] Reference 45. [k] Reference 23. [l] All-electron calculations adding g-functions, ref 15. [m] Dirac 4-component calculation, ref 24. [n] Reference 24. [o] Reference 16. [p] Approximate quadratic coupled-cluster calculation, ref 16.

the so-called ΔSCF method which carries out separate SCF (self-consistent field) calculations for the molecule and its ion. The An−O stretching force constants (k) (symmetric and antisymmetric) and the corresponding vibrational frequencies (ω) were determined from a mth-order polynomial fit to the energies of n points ($n > m$). The results of Mulliken population analysis are given in Table 2b.

Figure 2 illustrates the valence molecular orbital (MO) energy levels for the nonrelativistic and relativistic ground states of the AnO_2's, obtained by spin-restricted calculations. Mulliken populations (contributions) of the An-5f/6d/7s and O-2p orbitals are indicated in parentheses so as to assist in interpretation.

Since there have been many theoretical studies of isolated actinyls in the literature, our discussions here focus mainly on some special, important aspects of the results. To assess the accuracy of the present ADF method, some recent theoretical results[15,16,23−25,39] obtained from high-quality CI (configuration interaction), CC (coupled-cluster), and widely used B3LYP density-functional methods, are listed in Table 2a for comparison; they are all shown to be in good agreement with our results.

3.1.1. UO_2 and UO_2^{2+}. Nonrelativistically, the lowest energy electronic configuration for UO_2 is calculated to be $(\delta_u)^2$, a $^3\Sigma_g$ state. A previous nonrelativistic ADF calculation of UO_2 using a simple X_α potential, and without adding polarization functions, yielded a $(\delta_u)^1(\phi_u)^1 - {}^3H_g$ ground state. According to the present, more accurate ADF calculation, the ^3H_g state is about 0.2 eV higher in energy than $^3\Sigma_g$.

At the relativistic level, $(\sigma_g)^1(\phi_u)^1 - {}^3\Phi_u$ is the ground state, followed by $(\sigma_g)^1(\delta_u)^1 - {}^3\Delta_u$. Now the $(\delta_u)^2 - {}^3\Sigma_g$ state lies 0.85 eV above the ground state. Other CI, CC, and B3LYP calculations of UO_2 yield the same $^3\Phi_u$ ground state, but the orbital energy level diagram obtained with these methods is similar to our nonrelativistic one where σ_g is the LUMO+4.[25] Another notable feature of UO_2 is that for any given state, the relativistic bond length is consistently significantly greater than the nonrelativistic one, in contrast to the bond contraction typically found for other related compounds. The origin of this anomalous relativistic bond expansion was investigated by van Wezenbeek et al.[22] who ascribed it to the special semicore nature of the 6p shell in the U atom.

Our calculated first ionization potential (first IP) of UO_2 is 6.47 eV, comparable to the values obtained by the CI, CC, and B3LYP methods. The first IP of gas-phase UO_2 was previously measured using electron impact mass spectrometry at high temperature, and a value of 5.4 ± 0.1 eV was reported.[41] The same value was also obtained recently by Capone et al.[42] in a similar experiment. However, as pointed out by Gagliardi et al.,[39a] such high-temperature measurements may not give a

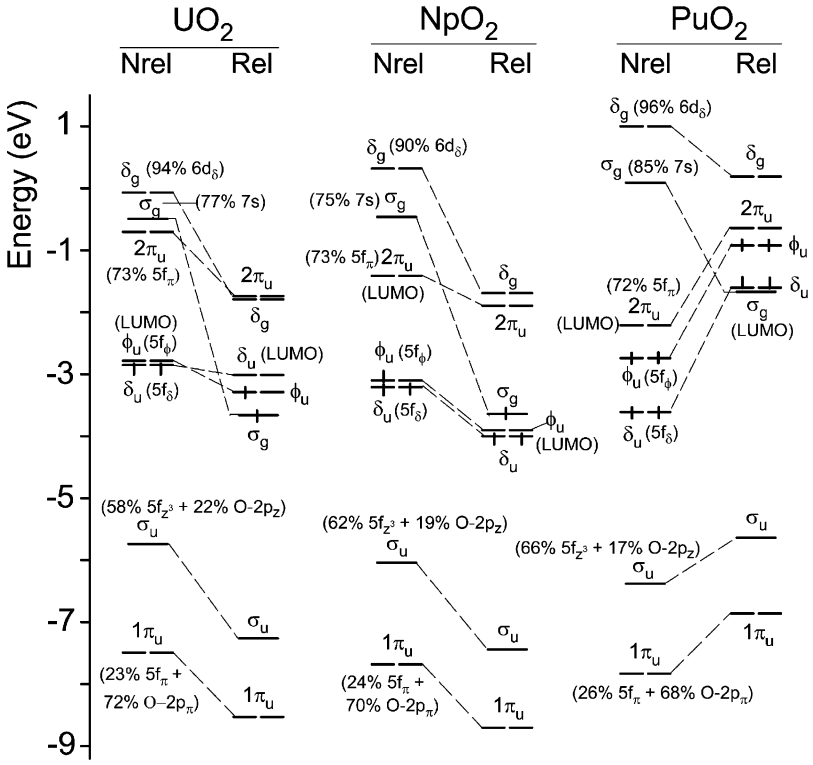

Figure 2. Orbital energy levels of AnO_2 (An = U, Np, Pu) at nonrelativistic (Nrel) and relativistic (Rel) levels. ($5f_\delta$ corresponds to $5f_{z(x^2-y^2)}/5f_{xyz}$, $5f_\phi$ to $5f_{x(x^2-3y^2)}/5f_{y(3x^2-y^2)}$, $5f_\pi$ to $5f_{z^2x}/5f_{z^2y}$, and $6d_\delta$ to $6d_{x^2-y^2}/6d_{xy}$.)

realistic first IP for this molecule since metastable, excited-state molecules are present in the vapor. Very recently, Heaven's group performed accurate determinations of IPs for UO_2 by using resonantly enhanced multiphoton ionization (REMPI) and mass-analyzed threshold ionization (MATI) techniques;[43] they obtained 6.19 eV for the first IP. Our calculated value is about 0.3 eV too large. The REMPI spectrum of UO_2 implies a $^3\Phi_u$ ground state for this molecule. The experimental prediction of the ground state is supported by the relativistic calculation. According to the calculation, the first electron is removed from σ_g, although this orbital is the HOMO−1; the IP from the HOMO ϕ_u is more than 2 eV greater. The second IP was found to be 14.92 eV, which is quite close to the value calculated by the CCSD/RPP (RPP = relativistic pseudopotential) method (15.05 eV).[44] The B3LYP calculations[25,39a] yielded a second IP of 15.3 eV, which is about 0.4 eV larger than our value. There has been a measurement of the second IP for UO_2 in the gas phase, and it was estimated to be 15.4 ± 2.6 eV through the thermodynamic data.[44] The experimental uncertainty is too large to judge the accuracy of the calculated values.

Only the antisymmetric stretching frequency of UO_2 can be compared to the experiment. The infrared value reported by Zhou et al.[25] is 915 cm^{-1} (for ^{16}O). Our calculated ω^{as} value comes out too large by about 30 cm^{-1}. The inclusion of SO coupling has an effect of −14 cm^{-1} and improves the vibrational frequency.

3.1.2. NpO_2 and NpO_2^{2+}. The nonrelativistic ground state of NpO_2, $(\delta_u)^2(\phi_u)^1 - {}^4\Phi_u$, corresponds to that of UO_2 by addition of one electron to ϕ_u. The relativistic effects again strongly stabilize the σ_g orbital and change the ground state to $(\delta_u)^2(\sigma_g)^1 - {}^4\Sigma_g$ or $(\delta_u)^1(\phi_u)^1(\sigma_g)^1 - {}^4H_g$; the latter configuration lies only 0.01 eV above the former, leaving the identity of the ground state in some doubt. In fact, the calculated energy of the $(\delta_u)^2(\phi_u)^1$ configuration is also close to that of $(\delta_u)^2(\sigma_g)$.[1] Compared to U, the larger nuclear charge in Np stabilizes the f orbitals so that the δ_u and ϕ_u orbitals lie below the σ_g level.

The Np−O bond length is shorter than that of U−O by 0.04 Å. Correspondingly, the Np−O force constant is 0.24 mdyn/Å larger than that of the U−O analogue. Similar to UO_2, the first ionization for NpO_2 also occurs from the σ_g orbital, and the calculated first IP of NpO_2 is nearly the same as that of UO_2. Concerning the second IP, which arises from a 5f orbital, the calculated value is larger for NpO_2 than for UO_2. In NpO_2^{2+}, the single outermost electron occupies the ϕ_u orbital; an internal redistribution of electrons takes place after two electrons are removed from NpO_2.

3.1.3. PuO_2 and PuO_2^{2+}. On the basis of the orbital energy level diagram in Figure 2, the nonrelativistic ground state of PuO_2 is clearly $(\delta_u)^2(\phi_u)^2 - {}^5\Sigma_g$; there are no other competing low-lying states. At the relativistic level, there is no change of the ground state, that is, the σ_g orbital in PuO_2 is no longer occupied even though it is strongly stabilized by relativistic effects. The trend in the electronic configuration from UO_2 to NpO_2 to PuO_2 shows a gradual stabilization of the 5f orbitals as one progresses to the right along the actinide sequence. In Figure 2 one may note that the σ_g orbital is located below the δ_u and ϕ_u levels. This placement may be attributed to a good deal of repulsion of the electrons in the tight 5f orbitals, which leads to large upward shift of the 5f levels. On the other hand, the gap between the δ_u and ϕ_u levels widens considerably in PuO_2.

While $R_{Np-O} < R_{U-O}$, R_{Pu-O} is even larger than R_{U-O}. The relatively long Pu−O bond length may be ascribed to the aforementioned large 5f−5f repulsion in PuO_2. The trend in the k_{An-O}'s is consistent with that in the R_{An-O}'s. In contrast to UO_2 and NpO_2, the effect of SO coupling is large for the antisymmetric force constant of PuO_2. The first ionization in PuO_2 occurs from the ϕ_u orbital, while the second ionization takes place from the lower δ_u orbital. Thus, PuO_2^{2+} has a $(\delta_u)^1(\phi_u)^1 - {}^3H_g$ ground state, different from that of the isoelectronic UO_2. Previous CASSCF and CISD calculations by Hillier et al.[23] yielded a $^3\Sigma_g$ ground state for PuO_2^{2+}. More recent CI and

TABLE 3: Calculated Relative Energies (E, eV) and An−O/N Bond Lengths ($R_{An-O/N}$, Å) for Selected Configurations of AnO_2AP (An = U, Np, Pu), at Nonrelativistic (Nrel) and Relativistic (Rel) Levels

		configuration	term	E	R_{An-O}	R_{An-N1}	R_{An-N2}
UO_2AP	Nrel	$(1b_{2g})^1(2a_{1u})^1$	$^3B_{2u}$	0	1.772	2.551	2.865
		$(1b_{2g})^1(2b_{1u})^1$	$^3B_{3u}$	0.06	1.772	2.558	2.861
		$(1b_{2g})^2$	$^1A_{1g}$	0.08	1.756	2.517	2.846
		$(1b_{2g})^1(b_{3u})^1$	$^3B_{1u}$	0.10	1.782	2.556	2.864
		$(1b_{2g})^1(b_{3g})^1$	$^3B_{1g}$	1.18	1.757	2.514	2.854
	Rel	$(1b_{2g})^2$	$^1A_{1g}$	0	1.791	2.464	2.768
		$(1b_{2g})^1(2b_{1u})^1$	$^3B_{3u}$	1.52	1.794	2.463	2.773
		$(1b_{2g})^1(2a_{1u})^1$	$^3B_{2u}$	1.95	1.803	2.493	2.795
		$(1b_{2g})^1(b_{3u})^1$	$^3B_{1u}$	2.07	1.845	2.498	2.803
NpO_2AP	Nrel	$(b_{2g})^1(2a_{1u})^1(b_{3u})^1$	$^4B_{1g}$	0	1.768	2.547	2.867
		$(b_{2g})^1(2a_{1u})^1(b_{1u})^1$	$^4B_{3g}$	0.25	1.751	2.547	2.864
		$(b_{2g})^2(2a_{1u})^1$	$^2A_{1u}$	0.60	1.740	2.504	2.857
		$(b_{2g})^2(b_{3u})^1$	$^2B_{3u}$	0.68	1.762	2.517	2.838
	Rel	$(b_{2g})^2(2a_{1u})^1$	$^2A_{1u}$	0	1.767	2.450	2.785
		$(b_{2g})^2(b_{3u})^1$	$^2B_{3u}$	0.09	1.786	2.452	2.768
		$(b_{2g})^2(2b_{1u})^1$	$^2B_{1u}$	0.09	1.765	2.464	2.776
		$(b_{2g})^1(2a_{1u})^1(b_{3u})^1$	$^4B_{1g}$	1.29	1.799	2.486	2.802
PuO_2AP	Nrel	$(b_{2g})^1(2a_{1u})^1(2b_{1u})^1(b_{3u})^1$	$^5A_{1u}$	0	1.748	2.544	2.869
		$(b_{2g})^2(2a_{1u})^1(b_{3u})^1$	$^3B_{3g}$	0.85	1.742	2.510	2.859
		$(b_{2g})^2(2a_{1u})^1(2b_{1u})^1$	$^3B_{1g}$	1.23	1.728	2.515	2.860
	Rel	$(b_{2g})^2(2a_{1u})^1(b_{3u})^1$	$^3B_{3g}$	0	1.765	2.434	2.775
		$(b_{2g})^2(2a_{1u})^1(b_{1u})^1$	$^3B_{1g}$	0.28	1.746	2.447	2.786
		$(b_{2g})^1(2a_{1u})^1(2b_{1u})^1(b_{3u})^1$	$^5A_{1u}$	0.72	1.779	2.477	2.788

B3LYP calculations by Maron et al.[16] and Ismail et al.[24] support our assignment of PuO_2^{2+} as ^3H_g. The calculated first and second IPs for PuO_2 are larger than the corresponding values of NpO_2. Capone et al.[42] also performed a mass spectrometric measurement for the first IP of PuO_2; they obtained 10.1 ± 0.1 eV, more than 3 eV higher than the calculated value of 6.92 eV. Such a large difference is unexpected, and more reliable experimental measurements are required to confirm the calculated value. Going from the neutral to a dicationic species, there is a large shortening of the Pu−O bond length, by 0.13 Å. The An−O bond lengths of AnO_2^{2+} vary in the monotonic order $R_{U-O} > R_{Np-O} > R_{Pu-O}$.

3.2. Actinyls within the Expanded Porphyrin. Table 3 presents the relative energies and optimized bond lengths for selected configurations of the AnO_2AP species, calculated at both nonrelativistic and relativistic levels. The geometry of each state was optimized under D_{2h} symmetry. The calculated properties of ground-state AnO_2AP are reported in Table 4, together with the results of UO_2TTAP. The $AnO_2^{0/2+}$−$AP^{0/2-}$ binding energy E_{bind} is defined as

$$-E_{bind} = E(AnO_2AP) - [E(AnO_2^{0/2+}) + E(AP^{0/2-})]$$

Since the dominant form of actinide in nuclear waste is the actinyl ion AnO_2^{2+},[45] we have therefore also evaluated binding energies between AnO_2^{2+} and AP^{2-}. We believe that the definition of binding energy as that between two neutral fragments may give a more realistic measure of the system stability. In addition to IPs, calculated electron affinities (EAs) are listed for AnO_2AP; [they are defined as EA = $E(X^-)$ − $E(X)$].

Both nonrelativistic and relativistic ground-state electronic structures of UO_2AP are illustrated in Figure 3, together with the electronic structure of UO_2TTAP for the sake of comparison. The corresponding electronic structures of NpO_2AP and PuO_2-AP are presented in Figure 4. For actinyl in the expanded porphyrin, the An-5f atomic orbitals split into the b_{3u}, $2a_{1u}$, $2b_{1u}$, and b_{2u} orbitals.

3.2.1. UO_2AP. Although the gap between the $1b_{2g}$ and $2a_{1u}$ orbitals is large, the nonrelativistic calculation yields a $(1b_{2g})^1(2a_{1u})^1$ − $^3B_{2u}$ ground state,that is, one electron is located in an AP orbital and the other resides in a U-5f orbital. The closed-shell state $^1A_{1g}$ with two electrons in $1b_{2g}$ is about 0.1 eV higher in energy. The three 5f-like orbitals, $2a_{1u}$, b_{3u}, and $2b_{1u}$, which are close in energy, generate three low-lying triplets in the energy range within 0.1 eV. After taking into account relativistic effects, which strongly destabilize f orbitals, the ground state of UO_2AP is clearly $(1b_{2g})^2$ − $^1A_{1g}$, and second lowest state $(1b_{2g})^1(2b_{1u})^1$ − $^3B_{3u}$ lies more than 1.5 eV above $^1A_{1g}$. For a given configuration, the relativistic U−O bond is longer than the nonrelativistic one. The trend is similar to that found for UO_2 or UO_2^{2+}. In contrast, the U−N bonds are significantly contracted by relativistic effects.

Considering the calculated properties of UO_2AP in its ground state (Table 4) more thoroughly, the U−O bond length is reduced by only 0.02 Å when UO_2 is coordinated with AP. If one considers UO_2^{2+} as coordinated with AP^{2-}, then R_{U-O} in UO_2AP is expanded by 0.07 Å. From the Mulliken population analysis, 1.03 e is transferred from UO_2 to AP, much less than 2 e, suggesting substantial UO_2−AP covalent character. The symmetric U−O force constants in UO_2 and UO_2AP are comparable, that is, the small decease in R_{U-O} does not result in an increase in $k_{U-O}^{(s)}$. However, $k_{U-O}^{(as)}$ in UO_2AP is notably smaller than in UO_2. The experimental value of $\omega_{U-O}^{(as)}$ is also available for UO_2TTAP,[4] which is 910 cm^{-1}, agreeing very well with the calculated values (915 cm^{-1} for UO_2AP and 916 cm^{-1} for UO_2TTAP).

The UO_2−AP binding energy is estimated to be 10.3 eV, where spin−orbit (SO) coupling effects contribute about 0.2 eV to E_{bind}. The large interaction between UO_2 and AP is consistent with the high stability of the complex: UO_2AP undergoes no apparent decomposition or demetalation up to 300 °C.[46] When considering the UO_2^{2+}−AP^{2-} interaction, the calculated binding energy of this definition is as large as 28.1 eV.

The calculated first and second IPs are 6.45 and 9.75 eV, respectively, both emanating from the HOMO $1b_{2g}$. The calculated EA is quite negative, −1.95 eV, indicating a strong attraction of an electron for the complex. The orbital that accepts the additional electron is the AP antibonding b_{3g}, although the latter is the LUMO+4 in the (relativistic) orbital energy level

TABLE 4: Calculated Properties of AnO_2AP (An = U, Np, Pu) and UO_2TTAP in Their Ground States (relativistic results)[a]

	UO_2AP $[(1b_{2g})^2]$	UO_2TTAP $[(1b_{2g})^2]$	NpO_2AP $[(b_{2g})^2(2a_{1u})^1]$	PuO_2AP $[(b_{2g})^2(2a_{1u})^1(b_{1u})^1]$
R_{An-O}, Å	1.791	1.790 (1.770)[b]	1.767	1.765
R_{An-N1}, Å	2.464	2.499 (2.418)	2.450	2.434
R_{An-N2}, Å	2.768	2.742 (2.740)	2.785	2.775
$k_{An-O}^{(s)}$, mdyn/Å	6.80	6.82	6.84	6.72
$\omega_{An-O}^{(s)}$, cm^{-1}	849	850	852	844
$k_{An-O}^{(as)}$, mdyn/Å	6.97	6.98	8.25	8.05
$\omega_{An-O}^{(as)}$, cm^{-1}	915	916 (910)	996	982
$E_{bind}(AnO_2-AP)$, eV	10.04	9.85	9.37	8.33
$E_{bind}^{SO}(AnO_2-AP)$, eV	10.25	10.03	9.54	8.59
$E_{bind}(AnO_2^{2+}-AP^{2-})$, eV	28.05	30.47	28.05	28.14
first IP, eV	**6.45** ($1b_{2g}$)	**5.54** ($1b_{2g}$)	**6.40** (b_{2g})	**6.38** (b_{2g})
			6.90 ($2a_{1u}$)	7.09 ($2a_{1u}$)
				7.47 (b_{3u})
second IP, eV	**9.75** ($1b_{2g}$)	**8.47** ($1b_{2g}$)	**9.64** (b_{2g})	**9.69** (b_{2g})
	10.19 ($1a_{1u}$)	9.23 ($1a_{1u}$)	9.98 ($2a_{1u}$)	10.31 ($2a_{1u}$)
				10.66 (b_{3u})
EA, eV	−**1.95** (b_{3g})	−**1.63** (b_{3g})	−**2.06** ($2b_{1u}$)	−**2.40** ($2b_{1u}$)
	−1.67 ($2b_{1u}$)	−1.34 ($2b_{1u}$)	−1.92 (b_{3u})	−1.89 (b_{3g})
	−1.22 ($2a_{1u}$)	−0.90 ($2a_{1u}$)	−1.90 (b_{3g})	−1.40 ($2a_{1u}$)
	−0.93 (b_{3u})	−0.64 (b_{3u})	−0.58 ($2a_{1u}$)	−0.78 (b_{3u})
An-6p, e	5.43	5.42	5.35	5.29
An-6d, e	1.64	1.67	1.56	1.46
An-5f, e	2.56	2.57	3.72	4.83
An-7s, e	0.00	0.00	0.00	0.00
Q_{An}, e	2.49	2.49	2.45	2.50
Q_{AnO2}, e	1.03	1.02	1.03	1.09

[a] R_{An-O}, R_{An-N1}, and R_{An-N2} are the An−O, An−N1, and An−N2 bond lengths, respectively; $k_{An-O}^{(s)}$ is the symmetric An−O force constant; $\omega_{An-O}^{(s)}$ is the symmetric An−O vibrational frequency; $k_{An-O}^{(as)}$ is the antisymmetric An−O force constant; $\omega_{An-O}^{(as)}$ is the antisymmetric An−O vibrational frequency; $E_{bind}(AnO_2-AP)$ is the binding energy between AnO_2 and AP; $E_{bind}^{SO}(AnO_2-AP)$ is the binding energy after spin−orbit (SO) correction; $E_{bind}(AnO_2^{2+}-AP^{2-})$ is the binding energy between AnO_2^{2+} and AP^{2-}; IP is the ionization potential; EA is the electron affinity; An-6p, ..., An-7s is the gross Mulliken population on the atomic orbital; Q_{An} is the Mulliken charge on An; Q_{AnO2} is the Mulliken charge on AnO_2. [b] Values in parentheses are experimental data from ref 4.

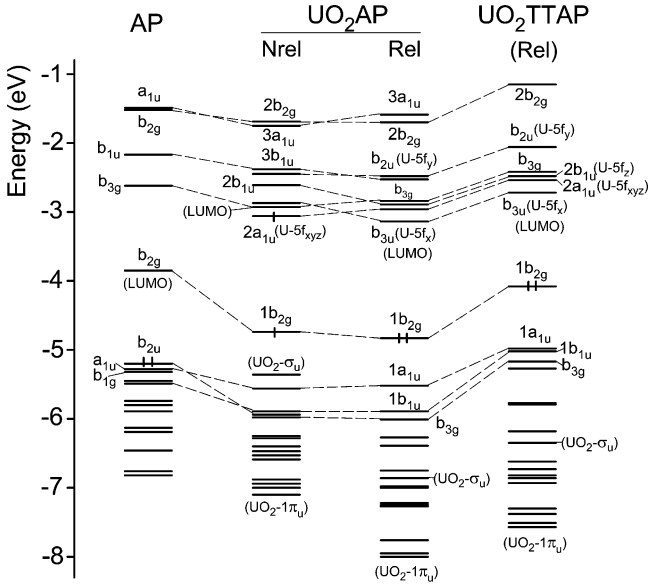

Figure 3. Orbital energy levels of UO_2AP at nonrelativistic (Nrel) and relativistic (Rel) levels, as well as the free-base AP and substituted UO_2TTAP. ($5f_x = 5f_{x(x^2-3y^2)}$, $5f_y = 5f_{y(3x^2-y^2)}$, and $5f_z = 5f_{z(x^2-y^2)}$.)

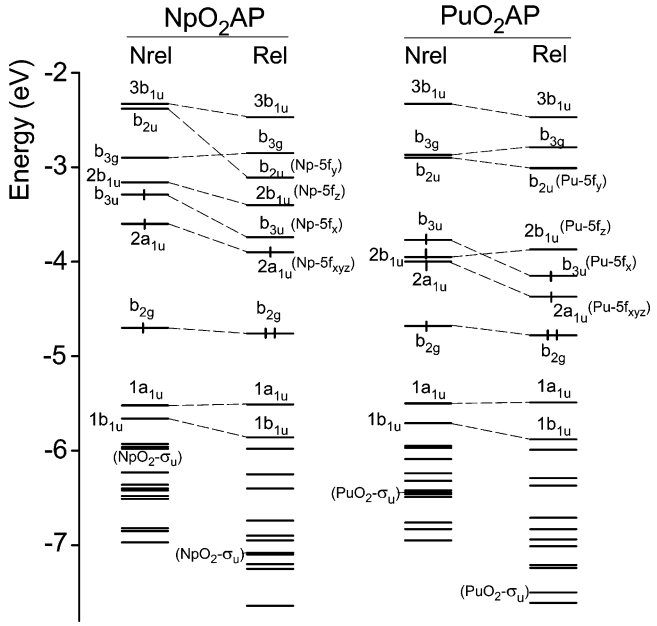

Figure 4. Orbital energy levels of NpO_2AP and PuO_2AP at nonrelativistic (Nrel) and relativistic (Rel) levels. ($5f_x = 5f_{x(x^2-3y^2)}$, $5f_y = 5f_{y(3x^2-y^2)}$, and $5f_z = 5f_{z(x^2-y^2)}$.)

diagram of UO_2AP. Addition of an electron to any of the lower-lying 5f-like orbitals (b_{3u}, $2a_{1u}$, or $2b_{1u}$) yields a smaller EA.

3.2.2. Effects of Substituents. The actinyl alaskaphyrins that have been synthesized actually contain four ethyl and four methoxy groups (see Figure 1) at the periphery of the macrocycle ring. To examine the effects of such peripheral substituents on the molecular properties, a more realistic UO_2TTAP system was examined explicitly. A comparison between the results for UO_2AP and UO_2TTAP is provided by Figure 3 and Table 4.

Both ethyl and methoxy are electron-donating groups, acting to shift the orbital energies up. These shifts are nearly uniform for the valence MOs, so the electronic structure of UO_2TTAP is qualitatively similar to that of UO_2AP. The U−O bond length and force constant remain nearly unchanged from UO_2AP to UO_2TTAP. In contrast, the changes in the U−N bond lengths are about 0.03 Å. The calculated U−O and U−N2 bond lengths in UO_2TTAP are very close to the X-ray crystal structure values.

A relatively large deviation of 0.08 Å is noted between the calculated and experimental U−N1 bond lengths. The substituents weaken the interaction of the actinyl with the macrocycle ring by 0.2 eV but do not influence the charge distribution on U and UO_2. Corresponding to the upshift of the valence MOs, the calculated IPs of UO_2TTAP are somewhat smaller than those of UO_2AP. The EA is diminished by 0.3 eV by the presence of the substituents.

3.2.3. NpO_2AP. It may be noted from Table 3 that, at the nonrelativistic level, the AP-b_{2g} orbital of NpO_2AP is singly occupied, similar to the case of UO_2AP; the other two outermost electrons occupy the 5f-like $2a_{1u}$ and b_{3u} orbitals, respectively. Relativistic effects destabilize the f orbitals and render one 5f electron transfer to the lower-lying AP-b_{2g} orbital. NpO_2AP has a $(b_{2g})^2(2a_{1u})^1 - {}^2A_{1u}$ ground state, followed by the states arising from the $(b_{2g})^2(b_{3u})^1$ and $(b_{2g})^2(2b_{1u})^1$ configurations; the latter two states are degenerate and ∼0.1 eV higher than the ground state.

Although there is 1.03 e charge transfer from NpO_2 to AP, the Np−O bond length in NpO_2AP is nearly equal to that in NpO_2, the difference being less than 0.01 Å. However the Np−O force constant is 0.3 mdyn/Å smaller in NpO_2AP than in NpO_2, in apparent contradiction to the bond length change. The first ionization arises from the AP b_{2g} although the HOMO $2a_{1u}$ lies some 0.8 eV higher. Ionization from $2a_{1u}$ requires 0.5 eV more than that from b_{2g}. The second ionization occurs from the b_{2g} orbital as well. It is no wonder then that the calculated IPs for NpO_2AP are comparable to those of UO_2AP. When one electron is added to NpO_2AP, it goes into a 5f-like $2b_{1u}$ orbital, different from the case of UO_2AP, likely due to the higher nuclear charge in Np (as compared to U) which lowers the energies of the 5f orbitals.

3.2.4. PuO_2AP. Similar to UO_2AP and NpO_2AP, the nonrelativistic ground state of PuO_2AP is also high spin, where the AP b_{2g} orbital is singly occupied. At the relativistic level, a pair of electrons occupy b_{2g}, and the lowest energy configuration is calculated to be $(b_{2g})^2(2a_{1u})^1(b_{3u})^1$, a ${}^3B_{3g}$ state. The state arising from $(b_{2g})^2(2a_{1u})^1(b_{1u})^1$ is 0.3 eV higher in energy. Compared to PuO_2, the Pu−O bond length in the coordinated complex is shortened significantly, by 0.08 Å. R_{Pu-O} in PuO_2AP is intermediate between those of PuO_2 and PuO_2^{2+}. Mulliken population analysis indicates 1.09 e charge transfer from PuO_2 to AP. Consistent with the bond shortening, the Pu−O force constant is greater in PuO_2AP than in PuO_2, somewhat different from the situations for An = U and Np.

Like UO_2AP and NpO_2AP, the first and second ionizations in PuO_2AP take place from the b_{2g} orbital. The IPs from the 5f-like orbitals in PuO_2AP are even larger than those in NpO_2AP, owing to a greater stabilization of the 5f orbitals in Pu than in Np. For the same reason, the calculated EA of PuO_2AP is significantly larger than that of NpO_2AP. This result is consistent with the experimental observation that Pu^{VI} can easily be reduced to Pu^{V} by accepting one electron.[12] On the other hand, it is easier to reduce the Np^{VI} complex than to reduce the corresponding U^{VI} species.[12] While the equatorial An−N bond lengths are similar in the three actinyl expanded porphyrins, there is a clear trend of decreasing AnO_2−AP binding energy in the order An = U > Np > Pu. It is interesting to note that when considering the interaction between AnO_2^{2+} and AP^{2-}, the calculated E_{bind} values are nearly the same among the three metals.

3.3. Hypothetical UO_2P and MAP (M = Ni, Zn). As pointed out in the Introduction, actinides do not form in-plane complexes with normal, tetradentate porphyrins, which is attributed to a poor match between the cation size and the macrocyclic cavity diameter. On the other hand, d-block transition metals show less tendency to form complexes with expanded porphyrins (except for some special cases[47]). To investigate the specific effects of the ring size and macrocycle rigidity on the metal−porphyrin bonding, calculations were performed for hypothetical UO_2P (P = porphine) and MAP (M = Ni, Zn) which contain smaller metals. The results are presented in Table 5, together with data for NiP and ZnP for comparison.

TABLE 5: Calculated Bond Lengths (R, Å) and Binding Energies (E_{bind}, eV) in UO_2P, MP, and MAP (M = Ni, Zn)

	P[a]	AP[a]	UO_2P	NiP	ZnP	NiAP	ZnAP
R_{U-O}			1.826				
R_{M-N1}	2.073 (Ct−N)	2.311 (Ct−N1)	2.253	1.969	2.062	2.075	2.094
R_{M-N2}		2.921 (Ct−N2)				2.990	2.982
E_{bind}[b]			7.88	10.13	6.52	6.05	3.85

[a] The distances between the center of the macrocycle ring (Ct) and the nitrogen atoms in P and AP (with no hydrogens in the cage) are also listed for comparison. [b] The binding energy is defined as the following: for UO_2P, $-E_{bind} = E(UO_2P) - [E(UO_2) + E(P)]$; for MP, $-E_{bind} = E(MP) - [E(M) + E(P)]$; for MAP, $-E_{bind} = E(MAP) - [E(M) + E(AP)]$.

The data indicate that the core size (indicated by the center−N distance R_{Ct-N}) in free-base porphyrin P (with no hydrogens in the cage) is about 2.07 Å. The central core of the hexaaza AP (R_{Ct-N1} = 2.31 Å, R_{Ct-N2} = 2.92 Å) is more than 12% larger than the tetraaza core of P. When P coordinates UO_2, its core expands to 2.25 Å, indicating a considerable strain on the P ligand. The UO_2−P binding energy is calculated to be 7.88 eV, much smaller than that of UO_2−AP. The change in macrocycle size also affects the U−O bond length; R_{U-O} in UO_2P is ∼0.04 Å longer than that in UO_2AP. In the case of the transition metals in AP, however, the expanded porphyrin provides a much weaker ligand field than does the normal porphyrin. The ionic radii of the transition metals are too small for them to form stable complexes with the large cyclic ligand.

Since the size of the porphinato core plays a pivotal role in controlling the spin state of transition metal porphyrins, the electronic structure of NiAP would be of interest and deserves a description here. The ground-state orbital energy level diagram of NiAP is illustrated in Figure 5, together with that of NiP for comparison. In NiP, the relatively small core size of P results in a large σ-donor interaction that elevates the metal $d_{x^2-y^2}$ orbital greatly; NiP hence has an unambiguous $(d_{xy})^2(d_{xz,yz})^4$ closed-shell ground state. Upon replacement of P by AP, the $d_{x^2-y^2}$ level is greatly lowered and the separations among the metal d orbitals in NiAP become small. In this case, one electron in d_{z^2} goes into $d_{x^2-y^2}$, and thus NiAP presents open shells.

4. Conclusions

Owing to large relativistic stabilization of the 7s-like orbital σ_g, UO_2 and NpO_2 have $(\sigma_g)^1(\phi_u)^1 - {}^3\Phi_u$ and $(\delta_u)^2(\sigma_g)^1 - {}^4\Sigma_g$ ground states, respectively. Without relativistic correction, the σ_g orbital is unoccupied due to its very high energy. In PuO_2, however, the four outermost electrons all occupy 5f-like orbitals, yielding a $(\delta_u)^2(\phi_u)^2 - {}^5\Sigma_g$ ground state. This result is attributed to a higher nuclear charge of Pu, which contracts the f orbitals more and lowers their energies. The nonrelativistic ground states of the AnO_2AP complexes are all high spin, where the AP HOMO b_{2g} is singly occupied. At the relativistic level, there are two electrons in b_{2g}, and the ground states are $(b_{2g})^2 - {}^1A_{1g}$, $(b_{2g})^2(2a_{1u})^1 - {}^2A_{1u}$, and $(b_{2g})^2(2a_{1u})^1(b_{3u})^1 - {}^3B_{3g}$ for UO_2AP,

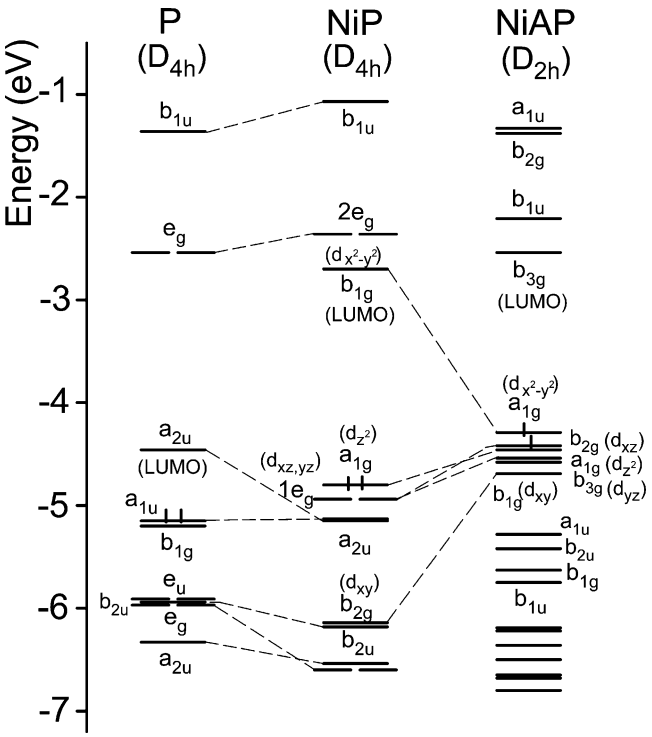

Figure 5. Orbital energy levels of free porphine (P) (on the left, with no H atoms in the porphyrin cage), NiP, and NiAP.

NpO_2AP, and PuO_2AP, respectively. Relativistic bond expansion of An−O is also found in AnO_2AP but is less pronounced than in AnO_2.

The bond of AnO_2−AP in the complex is characterized as strong and covalent. There is about 1.0−1.1 e charge transfer from AnO_2 to AP. The U−O and Np−O bond lengths are not influenced much by the AP coordination, but a relatively large bond shortening of Pu−O occurs when PuO_2 is coordinated with AP. The binding strength between AnO_2 and AP decreases in monotonic order UO_2−AP > NpO_2−AP > PuO_2−AP.

Both first and second ionizations of each AnO_2AP occur from the ring b_{2g} orbital, and so the calculated IPs are similar and independent of the metal. In the case of reduction, the situations are somewhat different for various systems. For UO_2AP, the electron adds to the AP antibonding b_{3g} orbital whereas the site of electron addition is a metal 5f-like orbital for the two heavier complexes. The calculated EA increases in the order UO_2AP < NpO_2AP < PuO_2AP, which indicates an increasing stability of An^V versus An^{VI} along the actinide series.

Finally the predicted spectroscopic constants for NpO_2, PuO_2, NpO_2AP, and PuO_2AP would aid in future spectroscopic studies of these molecules.

Acknowledgment. This work was supported by Grant DAAD19-99-1-0206 to S.S. from the Army Research Office.

References and Notes

(1) Leverd, P. C.; Dumazet-Bonnamoour, I.; Lamartine, R.; Nierlich, M. *Chem. Commun.* **2000**, 493.

(2) Clark, D. L.; Keogh, D. W.; Palmer, P. D.; Scott, B. L.; Tait, C. D. *Angew. Chem., Int. Ed.* **1998**, *37*, 164.

(3) (a) Burrel, A. K.; Hemmi, G.; Lynch, V.; Sessler, J. L. *J. Am. Chem. Soc.* **1991**, *113*, 4690. (b) Burell, A. K.; Cyr, M. J.; Lynch, V.; Sessler, J. L. *J. Chem. Soc., Chem. Commun.* **1991**, 1710.

(4) Sessler, J. L.; Mody, T. D.; Lynch, V. *Inorg. Chem.* **1992**, *31*, 529.

(5) Sessler, J. L.; Mody, T. D.; Dulay, M. T.; Espinoza, R.; Lynch, V. *Inorg. Chim. Acta* **1996**, *246*, 23.

(6) Sessler, J. L.; Gebauer, A.; Hoehner, M. C.; Lynch, V. *Chem. Commun.* **1998**, 1835.

(7) Sessler, J. L.; Tvermoes, N. A.; Davis, J.; Anzenbacher, P.; Jursikova, K.; Sato, W.; Seidel, D.; Lynch, V.; Black, C. B.; Try, A.; Andrioletti, B.; Hemmi, G.; Mody, T. D.; Magda, D. J.; Kral, V. *Pure Appl. Chem.* **1999**, *71*, 2009.

(8) Sessler, J. L.; Seidel, D.; Vivian, A. E.; Lynch, V.; Scott, B. L.; Keogh, D. W. *Angew. Chem., Int. Ed.* **2001**, *40*, 591.

(9) Hannah, S.; Seidel, D.; Sessler, J. L.; Lynch, V. *Inorg. Chim. Acta* **2001**, *317*, 211.

(10) Sessler, J. L.; Seidel, D.; Bucher, C.; Lynch, V. *Tetrahedron* **2001**, *57*, 3743.

(11) Sessler, J. L.; Vivian, A. E.; Seidel, D.; Burrell, A. K.; Hoehner, M.; Mody, T. D.; Gebauer, A.; Weghorn, S. J.; Lynch, V. *Coord. Chem. Rev.* **2001**, *216*−*217*, 411.

(12) Sessler, J. L.; Gorden, A. E. V.; Seidel, D.; Hannah, S.; Lynch, V.; Gordon, P. L.; Donohoe, R. J.; Tait, C. D.; Keogh, D. W. *Inorg. Chim. Acta* **2002**, *341*, 54.

(13) Girolami, G. S.; Milam, S. N.; Suslick, K. S. *Inorg. Chem.* **1987**, *26*, 343.

(14) Girolami, G. S.; Gorlin, P. A.; Milam, S. N.; Suslick, E. S.; Wilson, S. R. *J. Coord. Chem.* **1994**, *32*, 173.

(15) (a) Vallet, V.; Schimmelpfennig, B.; Maron, L.; Teichteil, C.; Leininger, T.; Gropen, O.; Grenthe, I.; Wahlgren, U. *Chem. Phys.* **1999**, *244*, 185. (b) Wahlgren, U.; Schimmelpfennig, B.; Jusuf, S. *Chem. Phys. Lett.* **1998**, *287*, 525.

(16) Maron, L.; Leininger, T.; Schimmelpfennig, B.; Vallet, V.; Heully, J.-L.; Teichteil, C.; Gropen, O.; Wahlgren, U. *Chem. Phys.* **1999**, *244*, 195.

(17) Wang, S.-G.; Pan, D.-K.; Schwarz, W. H. E. *J. Chem. Phys.* **1995**, *102*, 9296.

(18) Boettger, J. C.; Ray, A. K. *Int. J. Quantum Chem.* **2000**, *80*, 824.

(19) Boettger, J. C.; Ray, A. K. *Int. J. Quantum Chem.* **2002**, *90*, 1470.

(20) Pyykkö, P. *Inorg. Chim. Acta* **1987**, *139*, 243.

(21) Allen, G. C.; Baerends, E. J.; Vernooijs, P.; Dyke, J. M.; Ellis, A. M.; Feher, M.; Morris, A. *J. Chem. Phys.* **1988**, *89*, 5363.

(22) van Wezenbeek, E. M.; Baerends, E. J.; Snijders, J. G. *Theor. Chim. Acta* **1991**, *81*, 139.

(23) Craw, J. S.; Vincent, M. A.; Hillier, I. H.; Wallwork, A. L. *J. Phys. Chem.* **1995**, *99*, 10181.

(24) Ismail, N.; Heully, J.-L.; Saue, T.; Daudey, J.-P.; Marsden, C. J. *Chem. Phys. Lett.* **1999**, *300*, 296.

(25) Zhou, M.-F.; Andrews, L.; Ismail, N.; Marsden, C. *J. Phys. Chem. A* **2000**, *104*, 5495.

(26) Han, Y.-K.; Hirao, K. *J. Chem. Phys.* **2000**, *113*, 7345.

(27) de Jong, W. A.; Harrison, R. J.; Nichols, J. A.; Dixon, D. A. *Theor. Chem. Acc.* **2001**, *107*, 22.

(28) Szterenberg, L.; Latos-Grazynski, L. *J. Phys. Chem. A* **1999**, *103*, 3302.

(29) Baerends, E. J.; Ellis, D. E.; Ros, P. *Chem. Phys.* **1973**, *2*, 41.

(30) Versluis, L.; Ziegler, T. *J. Chem. Phys.* **1988**, *88*, 322.

(31) te Velde, G.; Baerends, E. J. *J. Comput. Phys.* **1992**, *99*, 84.

(32) Fonseca-Guerra, C.; Snijders, J. G.; te Velde, G.; Baerends, E. J. *Theor. Chem. Acc.* **1998**, *99*, 391.

(33) Vosko, S. H.; Wilk, L.; Nusair, M. *Can. J. Phys.* **1980**, *58*, 1200.

(34) Becke, A. D. *Phys. Rev. A* **1988**, *38*, 3098.

(35) Perdew, J. P. *Phys. Rev. B* **1986**, *33*, 8822.

(36) Johnson, B. G.; Gill, P. M. W.; Pople, J. A. *J. Chem. Phys.* **1993**, *98*, 5612.

(37) Li, J.; Schreckenbach, G.; Ziegler, T. *J. Am. Chem. Soc.* **1995**, *117*, 486.

(38) Ziegler, T.; Tschinke, V.; Baerends, E. J.; Snijders, J. G.; Ravenek, W. *J. Phys. Chem.* **1989**, *93*, 3050.

(39) (a) Gagliardi, L.; Roos, B. O.; Malmqvist, P.-Å.; Dyke, J. M. *J. Phys. Chem. A* **2001**, *105*, 10602. (b) Gagliardi, L.; Roos, B. O. *Chem. Phys. Lett.* **2000**, *331*, 229.

(40) Majumdar, D.; Balasubramanian, K.; Nitsche, H. *Chem. Phys. Lett.* **2002**, *361*, 143.

(41) Rauh, E. G.; Ackerman, R. J. *J. Chem. Phys.* **1974**, *60*, 1396.

(42) Capone, F.; Colle, Y.; Hiernaut, J. P.; Rouchi, C. *J. Phys. Chem. A* **1999**, *103*, 10899.

(43) Han, J.-D.; Kaledin, L. A.; Goncharov, V.; Komissarov, A. V.; Heaven, M. C. *J. Am. Chem. Soc.* **2003**, *125*, 7176.

(44) Cornehl, H. H.; Heinemann, C.; Marcalo, J.; de Matos, A. P.; Schwarz, H. *Angew. Chem., Int. Ed. Engl.* **1996**, *35*, 891.

(45) Clavaguéra-Sarrio, C.; Hoyan, S.; Ismail, N.; Marsden, C. J. *J. Phys. Chem. A* **2003**, *107*, 4515.

(46) Alexander, V. *Chem. Rev.* **1995**, *95*, 273.

(47) Hannah, S.; Lynch, V.; Guldi, D. M.; Gerasimchuk, N.; MacDonald, C. L. B.; Magda, D.; Sessler, J. L. *J. Am. Chem. Soc.* **2002**, *124*, 8416.